Research Article

Khursheed J. Ansari, Mohammad Izadi*, and Samad Noeiaghdam

Enhancing the accuracy and efficiency of two uniformly convergent numerical solvers for singularly perturbed parabolic convection–diffusion–reaction problems with two small parameters

https://doi.org/10.1515/dema-2023-0144
received January 18, 2023; accepted January 8, 2024

Abstract: This study is devoted to designing two hybrid computational algorithms to find approximate solutions for a class of singularly perturbed parabolic convection–diffusion–reaction problems with two small parameters. In our approaches, the time discretization is first performed by the well-known Rothe method and Taylor series procedures, which reduce the underlying model problem into a sequence of boundary value problems (BVPs). Hence, a matrix collocation technique based on novel shifted Delannoy functions (SDFs) is employed to solve each BVP at each time step. We show that our proposed hybrid approximate techniques are uniformly convergent in order $O(\Delta\tau^s + M^{-\frac{1}{2}})$ for $s = 1, 2$, where $\Delta\tau$ is the time step and M is the number of SDFs used in the approximation. Numerical simulations are performed to clarify the good alignment between numerical and theoretical findings. The computational results are more accurate as compared with those of existing numerical values in the literature.

Keywords: collocation points, convergent analysis, Delannoy functions, stability, Taylor expansion, Rothe method, singularly perturbed problem

MSC 2020: 65M70, 65N12, 41A10, 35B25

1 Introduction

There are lots of studies focusing on the numerical solutions of singularly perturbed convection–diffusion–reaction equations. The singular perturbations have appeared in control theory [1], hydrodynamics, fluid or gas dynamics, in the modeling of semiconductor devices [2], etc. For more details, see [3]. Numerical treatments of differential equations with small parameters typically lead not to satisfactory results. In fact, in the presence of these parameters, we have boundary layer regions in which the calculated solution varies rapidly

*** Corresponding author: Mohammad Izadi,** Department of Applied Mathematics, Faculty of Mathematics and Computer, Shahid Bahonar University of Kerman, Kerman, Iran, e-mail: izadi@uk.ac.ir
Khursheed J. Ansari: Department of Mathematics, College of Science, King Khalid University, Abha, 61413, Saudi Arabia, e-mail: ansari.jkhursheed@gmail.com
Samad Noeiaghdam: Industrial Mathematics Laboratory, Baikal School of BRICS, Irkutsk National Research Technical University, Irkutsk, 664074, Russia; Department of Applied Mathematics and Programming, South Ural State University, Lenin prospect 76, Chelyabinsk, 454080, Russia, e-mail: snoei@istu.edu, noiagdams@susu.ru

in order to satisfy the boundary condition. Such phenomena give rise to numerical cumbersomes and make the investigation of convergence analysis very difficult [4,5,7].

In this work, we aimed to solve 1-D singularly perturbed second-order parabolic partial differential equations with two hybrid approaches. To be more precise, we study the following convection–diffusion–reaction (CDR) model problems with two small parameters given by [6,7]:

$$\frac{\partial w}{\partial \tau}(x,\tau) - \varepsilon \frac{\partial^2 w}{\partial x^2}(x,\tau) - \mu B(x,\tau)\frac{\partial w}{\partial x}(x,\tau) + A(x,\tau)w(x,\tau) = h(x,\tau), (x,\tau) \in \Omega, \tag{1}$$

where $\Omega \coloneqq \Omega_x \times (0,T]$ and $\Omega_x \coloneqq (0,L)$ with $L > 0$. Here, we assume that the coefficients $A(x,\tau)$, $B(x,\tau)$, and $h(x,\tau)$ are sufficiently smooth real-valued functions. We suppose further $A(x,\tau)$ satisfies

$$A(x,\tau) > 0, \quad x \in \Omega_x. \tag{2}$$

Moreover, $0 < \mu \ll 1$ and $0 < \varepsilon \ll 1$ as the perturbation parameters are two small constant parameters. With (1), the following initial condition is given as:

$$w(x,0) = g(x), \quad x \in \bar{\Omega}_x \coloneqq [0,L], \tag{3}$$

and subject to the following two boundary conditions:

$$w(0,\tau) = a_0(\tau), \quad w(L,\tau) = a_L(\tau), \quad \tau \in [0,T], \tag{4}$$

where $a_0(\tau)$ and $a_L(\tau)$ are two given functions. We emphasize that the existence and uniqueness of the solution $w(x,\tau)$ of the aforementioned initial boundary value problem (BVP) are guaranteed if the data are sufficiently smooth and under some appropriate compatibility conditions (see [6,7,10] for details). On the other hand, this unique solution $w(x,\tau)$ exhibits two boundary layers at two extreme spatial points $x = 0, L$. To the best of our knowledge, only a few methods have been developed for (1) with initial and boundary conditions (3)–(4). In [6], a parameter-uniform computational algorithm was constructed, which is based on an upwind finite difference scheme and a suitable piecewise uniform mesh. Besides, a scheme for the numerical treatments of (1)–(4) is based on a moving mesh-adaptive strategy, which adapts meshes to boundary layers proposed in [7]. The authors also proved that the proposed method is ε-uniform convergent of order $O(M^{-1+q} + \Delta\tau)$ under two restrictive conditions $\varepsilon \geqslant \mu^2$ and $M^{-q} < C\Delta\tau$. Here, M is the number of spatial grid points, $\Delta\tau$ is the time step, and $0 < q < 1$ is a real number. In [8], the authors proposed a parameter-uniform computational scheme based on higher-order finite difference method (FDM) for the model (1). Finally, a mesh-free procedure based on local radial basis function and FDM was investigated in [9].

Over the past decades, rapid strides have been made to develop various analytical and numerical procedures for solving time-dependent singular perturbation problems and some related model problems. Among various available approaches, let us mention the followings. The method is based on implicit Euler in time and upwind scheme on a nonuniform spatial mesh proposed in [11]. The sinc-Galerkin procedure is presented in [5], and the technique of Richardson extrapolations was developed in [13]. In [12], the authors used the Rothe in temporal direction and B-spline collocation scheme on a Shishkin mesh in space. Similarly, a combination of Crank-Nicolson and exponentially fitted operator finite difference scheme as well as the hybrid Crank-Nicolson/redefined cubic B-spline finite element method (FEM) developed in [14,15] respectively. Moreover, an upwind method based on the fitted Shishkin mesh was first proposed in [16]. Second, a hybrid approach comprises the midpoint upwind and the central difference method developed in [16]. The authors in [17] first discretized the time by the implicit-trapezoidal technique, and then, a combination of the midpoint upwind and central difference methods is utilized for the spatial variable. The streamline diffusion FEM was investigated in [18–20] and the finite element schemes on Bakhalov-type meshes considered in [21,22]. An exponentially fitted approach with regard to the space direction and the Crank-Nicolson scheme with respect to the time variable was proposed in [23] on a uniform mesh. Furthermore, we may point out some other effective methods for solving these kinds of model problems given in [24–32].

The primary aim of this manuscript is to examine two combined computational schemes to attain approximate solutions of (1)–(4) accurately and more straightforwardly than to existing numerical procedures. First, the temporal discretization is carried out via the Rothe horizontal method of line and the Taylor expansion

series formula. Hence, a matrix collocation technique based on a novel set of orthogonal polynomials, which is called shifted Delannoy functions (SDFs), is applied to the spatial variable. Also, the convergence and error analysis of the proposed methods in each direction are investigated in detail. Hence, we prove that our proposed techniques are uniformly convergent with complexity $O(\Delta\tau^s + \frac{1}{\sqrt{M}})$, where $\Delta\tau$ is the time step and M is the number of SDFs. Here, $s = 1$ corresponds to the Rothe approach, while $s = 2$ is related to the Taylor method.

The plan of this manuscript is given as follows. In Section 2, some fundamental facts of Delannoy polynomials together with their proof of convergence in the (weighted) L_2 and L_∞ are given. Time marching algorithms based on the Rothe and Taylor series approaches are given next in Section 3. Then, an investigation of the stability together with error estimations is considered. Section 4 is devoted to the implementations of two hybrid Rothe/Taylor-Delannoy methods in detail. In Section 5, the validations of the presented techniques are shown by comparison with existing numerical models and computational experiments. Finally, the conclusion is brought in Section 6. Throughout this study, the constants C and C_1 are positive independent of ε, M, and R as the number of time intervals. They may not have the same value at each occurrence.

2 Delannoy functions: A shifted version

Many enumeration problems can be expressed in terms of Delannoy numbers $\mathbb{D}_{m,k}$, where $m, k \in \mathbb{N}$. We refer to [33–35] for more information. These numbers are related to the number of lattice paths from $(0, 0)$ to (m, m) in which the only allowed steps (jumps) are $(1, 0)$, $(0, 1)$, and $(1, 1)$. The (central) Delannoy numbers are given by the formula:

$$\mathbb{D}_{m,k} = \sum_{j=0}^{m} \binom{m}{j}\binom{k}{j} 2^j.$$

Based on the aforementioned description, we have the following definition related to $\mathbb{D}_m \equiv \mathbb{D}_{m,m}$:

Definition 2.1. The Delannoy polynomials are defined as:

$$\mathbb{D}_m(z) = \sum_{j=0}^{m} \binom{m}{j}\binom{m+j}{j} z^j, \quad m \in \mathbb{N}. \tag{5}$$

Clearly, we have $\mathbb{D}_0(z) = 1$ and $\mathbb{D}_1(z) = 1 + 2z$. Using the fact that $\mathbb{D}_m(z)$ coincides with the Legendre polynomials $L_m(2z + 1)$, we obtain the following recursive relation:

$$\mathbb{D}_m(z) = \frac{2m-1}{m}(2z+1)\mathbb{D}_{m-1}(z) - \frac{m-1}{m}\mathbb{D}_{m-2}(z), \quad m \geqslant 2. \tag{6}$$

Also, the following orthogonality condition holds

$$\int_{-1}^{0} \mathbb{D}_n(z)\mathbb{D}_m(z)w(z)\mathrm{d}z = \frac{1}{2m+1}\delta_{mn}, \tag{7}$$

with respect to the weight function $w(z) \equiv 1$. A simple calculation shows that these new polynomials satisfy the following differential equation:

$$z(z+1)\mathbb{D}''_m(z) + (2z+1)\mathbb{D}'_m(z) = m(m+1)\mathbb{D}_m(z). \tag{8}$$

Using the fact that the roots of the Legendre polynomials are located in $(-1, 1)$ [36, Thm. 62], we have the following observation:

Lemma 2.2. *All zeros of Delannoy polynomials are negative, simple, and lie in* $(-1, 0)$.

In applications, we are mainly interested in using the Delannoy functions on a positive interval $[0, L]$. Thus, the shifted version of Delannoy polynomials in Definition 2.1 is defined next:

Definition 2.3. The SDFs on $[0, L]$ are defined as:

$$\mathbb{D}^{\star}_{m}(x) = \mathbb{D}_{m}(z), \quad z = \frac{x}{L} - 1, \quad x \in [0, L]. \tag{9}$$

In the explicit form, according to Definition 2.1, we may write

$$\mathbb{D}^{\star}_{m}(x) = \sum_{j=0}^{m} L^{-j} \binom{m}{j} \binom{m+j}{j} (x - L)^{j}, \quad m \in \mathbb{N}. \tag{10}$$

Furthermore, the set of Delannoy polynomials $\{\mathbb{D}^{\star}_{m}(x)\}_{m=0}^{\infty}$ are satisfied in the relation:

$$\int_{0}^{L} \mathbb{D}^{\star}_{n}(x) \mathbb{D}^{\star}_{m}(x) w(x) \mathrm{d}x = \frac{L}{2m+1} \delta_{mn}. \tag{11}$$

2.1 Convergence and error analysis

A function $f(x) \in L_2(\Omega_x)$ can be represented as a linear combination of SDFs. Thus, we have

$$f(x) = \sum_{m=0}^{\infty} d_m \mathbb{D}^{\star}_{m}(x), \tag{12}$$

with the coefficients d_m, $m \geqslant 1$ being explicitly as:

$$d_m = \frac{2m+1}{L} \int_{0}^{L} \mathbb{D}^{\star}_{m}(x) f(x) \mathrm{d}x, \quad m = 1, 2, \ldots. \tag{13}$$

To proceed, we need the following results to estimate an upper bound for the coefficients d_m given in (13).

Lemma 2.4. *The following results are valid for the SDFs*:

(i) $\mathbb{D}^{\star}_{m}(0) = (-1)^m$, $\mathbb{D}^{\star}_{m}(L) = 1$, *and* $|\mathbb{D}^{\star}_{m}(x)| < 1$ *for* $0 < x < L$,

(ii) $\mathbb{D}^{\star}_{m}(x) = \frac{L}{2(2m+1)} \left(\frac{\mathrm{d}}{\mathrm{d}x} \mathbb{D}^{\star}_{m+1}(x) - \frac{\mathrm{d}}{\mathrm{d}x} \mathbb{D}^{\star}_{m-1}(x) \right)$,

(iii) $|\mathbb{D}^{\star}_{m}(x)| \leqslant \frac{L}{2} \frac{\sqrt{\pi}}{\sqrt{2mx(L-x)}}$, *for* $x \in (0, L)$.

Proof. The proof of i) is obtained by using the fact that the Legendre polynomials satisfy $L_m(1) = 1$ and $L_m(-1) = (-1)^m$. Also, we have $|L_m(z)| < 1$ for $-1 < z < 1$. The second one is deduced from the following relation [36]:

$$L_m(z) = \frac{1}{2m+1} (L'_{m+1}(z) - L'_{m-1}(z)), \tag{14}$$

and then using the transformation $z = 2x/L - 1$. To prove (iii), we apply the aforementioned change of variable to the following inequality, which is proved for the Legendre polynomials [36, Thm. 61]:

$$|L_m(z)| < \left[\frac{\pi}{2m(1 - z^2)} \right]^{\frac{1}{2}}, \quad -1 < z < 1. \qquad \square$$

It should be noted that the case (iii) provided an upper bound for the SDPs on $[0, L]$. We use this fact to prove that the infinite expansion series (12) is uniformly convergent.

Theorem 2.5. *Suppose that a given function* $f \in L_2(\Omega_x) \cap C^2(\bar{\Omega}_x)$ *can be written as* (12) *and* $M_2 = \max_{x\in\Omega_x}|f^{(2)}(x)|$. *Then, the series in* (12) *is uniformly convergent. Moreover, the following upper bound is valid for the coefficients* d_m *in* (13) *as*:

$$|d_m| \leqslant Cm^{-\frac{3}{2}}, \quad m > 3, \tag{15}$$

where $C = \frac{1}{2}\pi\sqrt{\pi}L^2M_2$.

Proof. We start with relation (ii) in Lemma 2.4 to arrive at:

$$I \coloneqq \int_0^L \mathbb{D}_m^\star(x)f(x)\mathrm{d}x = \frac{L}{2(2m+1)}\left[\int_0^L \frac{\mathrm{d}}{\mathrm{d}x}\mathbb{D}_{m+1}^\star(x)f(x)\mathrm{d}x - \int_0^L \frac{\mathrm{d}}{\mathrm{d}x}\mathbb{D}_{m-1}^\star(x)f(x)\mathrm{d}x\right]. \tag{16}$$

Applying the integration by parts (IP) to both integrals on the right-hand side and using the relations (i) in Lemma 2.4 reveal that

$$\int_0^L \frac{\mathrm{d}}{\mathrm{d}x}\mathbb{D}_s^\star(x)f(x)\mathrm{d}x = f(L) + (-1)^{s+1}f(0) - \int_0^L \mathbb{D}_s^\star(x)f'(x)\mathrm{d}x, \quad s = m \pm 1.$$

By inserting the former relations into (16) and canceling the similar terms, we find out

$$I = \frac{L}{2(2m+1)}\left[\int_0^L \mathbb{D}_{m-1}^\star(x)f'(x)\mathrm{d}x - \int_0^L \mathbb{D}_{m+1}^\star(x)f'(x)\mathrm{d}x\right]. \tag{17}$$

Using the relation (ii) in Lemma 2.4 for $m \to m \pm 1$ in the aforementioned relation (17), we obtain

$$\begin{aligned} I = \frac{L}{2(2m+1)}\Bigg[&\int_0^L \frac{L}{2(2m-1)}\left(\frac{\mathrm{d}}{\mathrm{d}x}\mathbb{D}_m^\star(x) - \frac{\mathrm{d}}{\mathrm{d}x}\mathbb{D}_{m-2}^\star(x)\right)f'(x)\mathrm{d}x \\ &- \int_0^L \frac{L}{2(2m+3)}\left(\frac{\mathrm{d}}{\mathrm{d}x}\mathbb{D}_{m+2}^\star(x) - \frac{\mathrm{d}}{\mathrm{d}x}\mathbb{D}_m^\star(x)\right)f'(x)\mathrm{d}x\Bigg]. \end{aligned}$$

By repeating the IP in the last terms and then simplifying, we obtain

$$I = \frac{L^2}{4(4m^2-1)}\int_0^L (\mathbb{D}_{m-2}^\star(x) - \mathbb{D}_m^\star(x))f''(x)\mathrm{d}x - \frac{L^2}{4(2m+1)(2m+3)}\int_0^L (\mathbb{D}_m^\star(x) - \mathbb{D}_{m+2}^\star(x))f''(x)\mathrm{d}x.$$

Therefore, using the triangle inequality, we obtain

$$|d_m| = \frac{2m+1}{L}|I| \leqslant \frac{LM_2}{4(2m-1)}\int_0^L (|\mathbb{D}_{m-2}^\star(x)| + |\mathbb{D}_m^\star(x)|)\mathrm{d}x + \frac{LM_2}{4(2m+3)}\int_0^L (|\mathbb{D}_m^\star(x)| + |\mathbb{D}_{m+2}^\star(x)|)\mathrm{d}x.$$

Now, we apply the third inequality (iii) in Lemma 2.4 to arrive at

$$\begin{aligned} |d_m| &\leqslant \frac{LM_2}{4(2m-1)}\int_0^L \frac{1}{\sqrt{x(L-x)}}\left(\frac{L}{2}\sqrt{\frac{\pi}{2(m-2)}} + \frac{L}{2}\sqrt{\frac{\pi}{2m}}\right)\mathrm{d}x \\ &\quad + \frac{LM_2}{4(2m+3)}\int_0^L \frac{1}{\sqrt{x(L-x)}}\left(\frac{L}{2}\sqrt{\frac{\pi}{2m}} + \frac{L}{2}\sqrt{\frac{\pi}{2(m+2)}}\right)\mathrm{d}x \\ &\leqslant \frac{2L^2M_2}{4(2m-1)}\sqrt{\frac{\pi}{2(m-2)}}\int_0^L \frac{\mathrm{d}x}{\sqrt{x(L-x)}}. \end{aligned}$$

It is not a difficult task to show that

$$\int_0^L \frac{\mathrm{d}x}{\sqrt{x(L-x)}} = \pi.$$

By utilizing the obvious inequality $2m - 1 > 2m - 4$, we obtain

$$|d_m| \leqslant \frac{1}{2}L^2 M_2 \left(\frac{\pi}{2m-4}\right)^{3/2}, \quad m \geqslant 3. \tag{18}$$

Clearly, for $m > 3$, we have $2m - 4 > m$. Thus, the proof is complete. □

Instead of infinite series solution given in (12), we consider practically a truncated series solution that consists of $(M + 1)$ Delannoy functions in the form:

$$f(x) \approx f_M(x) \coloneqq \sum_{m=0}^{M} d_m \mathbb{D}_m^*(x). \tag{19}$$

Let us denote the error between two consecutive approximations f_M and f_{M+1} by:

$$e_M(x) \coloneqq f_{M+1}(x) - f_M(x).$$

Furthermore, $\|g\|_2$ represents the (weighted) L_2 norm on Ω_x with regard to the weight function $w(x) = 1$. The next theorem gives us an error estimation for the error e_M.

Theorem 2.6. *Under the hypothesis of Theorem* 2.5, *the following error estimate holds*

$$\|e_M(x)\|_2 = O(M^{-2}).$$

Proof. According to the definition of error and (19), we obtain

$$\begin{aligned}
\|e_M(x)\|_2 &= \|f_{M+1}(x) - f_M(x)\|_2 \\
&= \left\| \sum_{m=0}^{M+1} d_m \mathbb{D}_m^*(x) - \sum_{m=0}^{M} d_m \mathbb{D}_m^*(x) \right\|_2 \\
&= \|d_{M+1}\mathbb{D}_{M+1}^*(x)\|_2 \\
&= |d_{M+1}| \|\mathbb{D}_{M+1}^*(x)\|_2.
\end{aligned}$$

Now, we utilize the orthogonality condition (11) and the result of Theorem 2.5 to obtain

$$\begin{aligned}
\|e_M(x)\|_2 &= |d_{M+1}| \sqrt{\frac{L}{2M+3}} \\
&< C(M+1)^{-\frac{3}{2}} \frac{L^{\frac{1}{2}}}{\sqrt{2M+3}} \\
&= O(M^{-2}).
\end{aligned}$$

□

Finally, we derive an upper bound for the (global) error between the infinite series expansion of $f(x)$ in (12) and its truncated series expansion $f_M(x)$ in (19). To continue, we define $E_M(x) = f(x) - f_M(x)$.

Theorem 2.7. *Suppose that* $f(x)$ *satisfies the hypothesis of Theorem* 2.5 *and* $E_M(x) = \sum_{m=M+1}^{\infty} d_m \mathbb{D}_m^*(x)$ *denotes the global error. Then, we have an error estimate for* $E_M(x)$ *in the* L_∞ *norm as*:

$$\|E_M\|_\infty \leqslant C_1 M^{-\frac{1}{2}}, \quad C_1 \coloneqq 2C. \tag{20}$$

Proof. By utilizing Lemma 2.4, part (i) together with the result of Theorem 2.5 reveals that

$$|E_M(x)| \leqslant \sum_{m=M+1}^{\infty} |d_m| |\mathbb{D}_m^*(x)| \leqslant \sum_{m=M+1}^{\infty} |d_m| \leqslant C \sum_{m=M+1}^{\infty} \frac{1}{m^{\frac{3}{2}}}.$$

Now, we use the well-known integral test, which says that

$$\sum_{m=M+1}^{\infty} \frac{1}{m^{\frac{3}{2}}} \leqslant \int_{M}^{\infty} y^{-\frac{3}{2}} \mathrm{d}y = \frac{2}{\sqrt{M}}.$$

Thus, the proof is completed by taking maximum over all $x \in \Omega_x$. □

3 Time advancement methodologies

Here, we propose two time-marching schemes to discretize the parabolic CDR equation (1). To this end, we first employ the Rothe method [37,38] as a first-order accurate procedure and we then consider the Taylor series formula to obtain a second-order accuracy in time (see [39–41]).

Let $\{\tau_r\}_{r=0}^{R}$ be a partitioning of the interval $[0, T]$ into R uniform subintervals $R_r := [\tau_{r-1}, \tau_r]$ for $r = 1, 2, \ldots, R$. Here, the grid points and the time step are given by:

$$\tau_0 = 0 < \tau_1 = \Delta\tau < \ldots < \tau_R = R\Delta\tau = T, \quad \Delta\tau = \tau_r - \tau_{r-1}.$$

In the sequel, we use the symbol w_r to show the approximate solution at time level τ_r for $r = 1, 2, \ldots, R$, i.e., $w_r(x) := w(x, \tau_r)$.

3.1 Rothe first-order approach

The idea of Rothe technique consists of replacing the time derivative at the fixed points $\tau_r = r\Delta\tau$ by the following difference formula:

$$\frac{\partial w}{\partial \tau}(x, \tau_r) \approx \frac{w_r(x) - w_{r-1}(x)}{\Delta\tau}. \tag{21}$$

Moreover, the other x-derivatives can be expressed as:

$$w_r'(x) := \frac{\partial w}{\partial x}(x, \tau_r), \quad w_r''(x) := \frac{\partial^2 w}{\partial x^2}(x, \tau_r).$$

By replacing all terms in relation (1) by the aforementioned approximations at time level τ_r, we obtain the following BVPs:

$$\begin{cases} \dfrac{w_r(x) - w_{r-1}(x)}{\Delta\tau} - \varepsilon w_r''(x) - \mu B_r(x) w_r' + A_r(x) w_r(x) = h_r(x), \\ w_r(0) = a_0(\tau_r) := a_0^r, \\ w_r(L) = a_L(\tau_r) := a_L^r, \end{cases} \qquad r = 1, 2, \ldots, R,$$

where $A_r(x) = A(x, \tau_r)$, $B_r(x) = B(x, \tau_r)$, and $h_r(x) = h(x, \tau_r)$. After some manipulations, we rewrite the foregoing BVPs elegantly as:

$$\begin{cases} (1 + \Delta\tau A_r(x)) w_r(x) - \Delta\tau\mu B_r(x) w_r'(x) - \varepsilon\Delta\tau w_r''(x) = \Delta\tau h_r(x) + w_{r-1}(x), x \in \Omega_x, \\ w_r(0) = a_0^r, \\ w_r(L) = a_L^r, \end{cases} \tag{22}$$

for $r = 1, 2, \ldots, R$ and using the starting function $w_0(x) = g(x)$ as the given initial condition for the model Problem (1). If we solve the BVPs (22) subsequently, the functions $w_1(x)$, $w_2(x), \ldots w_R(x)$ are obtained. Hence, one can construct the so-called *Rothe functions* $W_1(x, \tau)$ in the whole domain Ω as:

$$W_1(x, \tau) = w_{r-1}(x) + \frac{w_r(x) - w_{r-1}(x)}{\Delta\tau}(\tau - \tau_{r-1}),$$

on the subinterval R_r for $r = 1, 2, \ldots, R$. Clearly, the constructed $W_1(x, \tau)$ is a piecewise function with respect to τ for every fixed x. By repeating the aforementioned approach with time steps $\Delta\tau/2, \Delta\tau/4, \Delta\tau/8, \ldots$, we obtain a sequence of related Rothe functions $\{W_m(x, \tau)\}_{m=1}^{\infty}$. Our expectation is that this sequence is convergent towards the true solution $w(x, \tau)$ of the original equation (1).

3.2 Taylor second-order approach

To proceed, we first substitute $\tau = \tau_r$ at the original equation (1) to obtain

$$\frac{\partial w_r}{\partial \tau} = \varepsilon \frac{\partial^2 w_r}{\partial x^2} + \mu B_r(x) \frac{\partial w_r}{\partial x} - A_r(x) w_r + h_r(x). \tag{23}$$

By means of the Taylor formula for w_r, we obtain

$$\frac{\partial w_r}{\partial \tau} = \frac{w_{r+1} - w_r}{\Delta\tau} - \frac{\Delta\tau}{2} \frac{\partial^2 w_r}{\partial \tau^2} + O(\Delta\tau^2). \tag{24}$$

We now differentiate (1) with regard to time variable τ followed by evaluating the resulting equation at τ_r to obtain

$$\frac{\partial^2 w_r}{\partial \tau^2} = \varepsilon \frac{\partial^2}{\partial x^2}\left(\frac{\partial w_r}{\partial \tau}\right) + \mu\left[\frac{\partial B_r}{\partial \tau}\frac{\partial w_r}{\partial x} + B_r(x)\frac{\partial}{\partial x}\left(\frac{\partial w_r}{\partial \tau}\right)\right] - \frac{\partial A_r}{\partial \tau} w_r(x) - A_r(x)\frac{\partial w_r}{\partial \tau} + \frac{\partial h_r}{\partial \tau}.$$

We now exploit the difference quotient $\frac{h_{r+1} - h_r}{\Delta\tau}$ instead of $\frac{\partial h_r}{\partial \tau}$ in the former relation. After multiplying both sides of the resulting relation by $\Delta\tau$, we obtain

$$\begin{aligned} \Delta\tau \frac{\partial^2 w_r}{\partial \tau^2} = \varepsilon\left(\frac{\partial^2 w_{r+1}}{\partial x^2} - \frac{\partial^2 w_r}{\partial x^2}\right) + \mu(B_{r+1} - B_r)\frac{\partial w_r}{\partial x} + \mu B_r(x)\left(\frac{\partial w_{r+1}}{\partial x} - \frac{\partial w_r}{\partial x}\right) \\ - (A_{r+1} - A_r) w_r(x) - A_r(x)(w_{r+1} - w_r) + h_{r+1} - h_r. \end{aligned} \tag{25}$$

We now come back to relation (24). On the left-hand side, we use relation (23) for the term $\frac{\partial w_r}{\partial \tau}$. On the right-hand side, we place $\Delta\tau \frac{\partial^2 w_r}{\partial \tau^2}$ via relation (25). After simplifying and then multiplying by $2\Delta\tau$, we arrive at the time discretized equation for (1) with second-order accuracy. Consequently, we obtain the following differential equation of second order as:

$$\sigma_{2,r-1}(x) w_r''(x) + \sigma_{1,r-1}(x) w_r'(x) + \sigma_{0,r-1}(x) w_r(x) = H_{r-1}(x), \quad x \in \Omega_x, \tag{26}$$

for $r = 1, 2, \ldots, R$. Here, the related coefficients are given by:

$$\begin{aligned} &\sigma_{2,r-1}(x) \coloneqq -\varepsilon\Delta\tau, \quad \sigma_{1,r-1}(x) \coloneqq -\mu\Delta\tau B_{r-1}(x), \quad \sigma_{0,r-1}(x) \coloneqq 2 + \Delta\tau A_{r-1}(x), \\ &H_{r-1}(x) \coloneqq [2 - \Delta\tau A_r(x)] w_{r-1}(x) + \Delta\tau(h_r + h_{r-1}) + \Delta\tau\varepsilon w_{r-1}''(x) + \mu\Delta\tau B_r(x) w_{r-1}'(x). \end{aligned}$$

Contrary to the Rothe method, in order to solve the system of linear equations (26), we require to have the initial condition $w_0(x) = g(x)$ as well as the first- and second-order derivatives. At every time step τ_r, the boundary conditions (4) at $x = 0, L$ are converted as:

$$w_r(0) \coloneqq a_0^r = a_0(\tau_r), \quad w_r(L) \coloneqq a_L^r = a_L(\tau_r), \quad r = 1, 2, \ldots, R. \tag{27}$$

3.3 Stability and error estimate in time

We now investigate the stability and convergence analysis of the discretized equation (26) and will prove its second-order accuracy. Similar techniques can be applied to establish the first-order accuracy of model (22). To proceed, we introduce the linear operator $\mathcal{L}_\varepsilon$ related to (26) as:

$$\mathcal{L}_\varepsilon[w_r](x) \coloneqq -\varepsilon \frac{\mathrm{d}^2}{\mathrm{d}x^2} w_r(x) - \mu B_{r-1}(x) \frac{\mathrm{d}}{\mathrm{d}x} w_r(x) + \left(\frac{2}{\Delta\tau} + A_{r-1}(x)\right) w_r(x).$$

Thus, we rewrite the relation (26) in a compact form:

$$\mathcal{L}_\varepsilon[w_r](x) = H_{r-1}(x), \quad x \in \Omega_x, \tag{28}$$

together with the following initial and boundary conditions:

$$w_0(x) = g(x), \quad w_r(0) = a_0^r, \quad w_r(L) = a_L^r, \tag{29}$$

for $r = 1, 2, \ldots, R$, and we also have

$$H_{r-1}(x) \coloneqq \left(\frac{2}{\Delta\tau} - A_r(x)\right) w_{r-1}(x) + \varepsilon w''_{r-1}(x) + \mu B_r(x) w'_{r-1}(x) + h_r(x) + h_{r-1}(x).$$

As mentioned earlier, the symbol $w_r(x) \approx w(x, \tau_r)$ denotes the approximate solution of (28) at time level τ_r.

Next, we state a theorem on the maximum principle for the operator $\mathcal{L}_\varepsilon$ as follows. The following maximum principle [42] holds for $\mathcal{L}_\varepsilon$.

Lemma 3.1. (Semi-discrete maximum principle) *Let assume that function $v \in C^2(\bar{\Omega}_x)$ satisfies $v(0) \geqslant 0$ and $v(L) \geqslant 0$. If $\mathcal{L}_\varepsilon[v](x) \geqslant 0$ for all $x \in \Omega_x$, then $v(x) \geqslant 0$ for all $x \in \bar{\Omega}_x$.*

Proof. The proof is done by contradiction. Let suppose that $x^\star$ be a point such that $v(x^\star) \coloneqq \min_{x \in \bar{\Omega}_x} v(x)$ and $v(x^\star) < 0$. By the assumptions, $x^\star \neq 0, L$. This implies that $v'(x^\star) = 0$ and $v''(x^\star) > 0$. Now, we have

$$\mathcal{L}_\varepsilon[v](x^\star) = -\varepsilon v''(x^\star) + \left(\frac{2}{\Delta\tau} + A_r(x^\star)\right) v(x^\star) < 0,$$

since $A_r(x^\star) > 0$ due to the constraint (2) we have assumed. This contradicts the hypothesis, and one concludes that $v(x^\star) > 0$. Therefore, our conclusion is that $v(x) \geqslant 0$ for all $x \in \bar{\Omega}_x$. □

Due to the fact that the operator $\mathcal{L}_\varepsilon$ in (28) satisfies in a maximum principle, the immediate conclusion is that the semi-discretized method (28)–(29) is stable in the following sense [11].

Corollary 3.2. (Stability) *The following stability estimate holds*

$$\|\mathcal{L}_\varepsilon^{-1}\|_\infty \leqslant C, \tag{30}$$

where C is a constant (independent of $\Delta\tau$ and ε).

The uniform convergence properties of semi-discretized method (28)–(29) is our next aim. To this end, we define the local truncation error (LTE) between $w_r(x)$ and true solution $w(x, \tau_r)$ as:

$$e_r(x) \coloneqq w(x, \tau_r) - w_r(x), \quad x \in \Omega_x.$$

Lemma 3.3. (Local error estimate [LEE]) *If there is a constant C such that*

$$\left| \frac{\partial^k w(x, \tau)}{\partial \tau^k} \right| \leqslant C, \quad \forall (x, \tau) \in \bar{\Omega}_x \times [0, T], \quad k = 0, 1, 2, 3,$$

then the LEE in the temporal direction satisfies

$$\|e_r\|_\infty = O(\Delta\tau^3). \tag{31}$$

Proof. We now rewrite Relation (28) in a new formulation as:

$$\begin{aligned} w_{r-1}(x) = w_r(x) - \frac{\Delta\tau}{2}[&\varepsilon(w''_{r-1}(x) + w''_r(x)) + \mu(B_{r-1}(x) w'_r(x) + B_r(x) w'_{r-1}(x)) \\ &- (A_{r-1}(x) w_r(x) + A_r(x) w_{r-1}(x)) + h_r(x) + h_{r-1}(x)]. \end{aligned} \tag{32}$$

Let $w(x, \tau)$ be the smooth solution of the original equation (1). By using the Taylor formula with integral remainder, we have

$$w(x, \tau_{r-1}) = w(x, \tau_r) - \Delta\tau w_\tau(x, \tau_r) + \frac{\Delta\tau^2}{2} w_{\tau\tau}(x, \tau_r) + \frac{1}{2}\int_{\tau_r}^{\tau_{r-1}} (\tau_{r-1} - \xi)^2 \frac{\partial^3 w}{\partial \tau^3}(x, \xi) \mathrm{d}\xi. \tag{33}$$

We now utilize expression (23) with $w(x, \tau_r)$ instead of $w_r(x)$ to obtain

$$w_\tau(x, \tau_r) = \varepsilon \frac{\partial^2 w(x, \tau_r)}{\partial x^2} + \mu B_r(x) \frac{\partial w(x, \tau_r)}{\partial x} - A_r(x) w(x, \tau_r) + h_r(x). \tag{34}$$

For the second-order derivative $w_{\tau\tau}(x, \tau_r)$, we use (25) except that on the right-hand side, we utilize the backward difference formula rather than forward one to obtain

$$\begin{aligned} \Delta\tau w_{\tau\tau}(x, \tau_r) = \varepsilon &\left(\frac{\partial^2 w(x, \tau_r)}{\partial x^2} - \frac{\partial^2 w(x, \tau_{r-1})}{\partial x^2} \right) + \mu(B_r(x) - B_{r-1}(x)) \frac{\partial w(x, \tau_r)}{\partial x} \\ &+ \mu B_r(x) \left(\frac{\partial w(x, \tau_r)}{\partial x} - \frac{\partial w(x, \tau_{r-1})}{\partial x} \right) - (A_r - A_{r-1}) w(x, \tau_r) \\ &- A_r(x)(w(x, \tau_r) - w(x, \tau_{r-1})) + h_r(x) - h_{r-1}(x). \end{aligned} \tag{35}$$

The next task is to substitute two forgoing Relations (34) and (35) into (33). Some simplifications give us

$$\begin{aligned} w(x, \tau_{r-1}) = w(x, \tau_r) &- \frac{\varepsilon\Delta\tau}{2}(w_{xx}(x, \tau_r) + w_{xx}(x, \tau_{r-1})) - \frac{\mu\Delta\tau}{2}(B_{r-1} w_x(x, \tau_r) + B_r w_x(x, \tau_{r-1})) \\ &+ \frac{\Delta\tau}{2}(A_{r-1} w(x, \tau_r) + A_r w(x, \tau_{r-1})) - \frac{\Delta\tau}{2}(h(x, \tau_r) + h(x, \tau_{r-1})) + O(\Delta\tau^3). \end{aligned} \tag{36}$$

We now subtract Relation (36) from (32). Consequently, we find that the LTE satisfies in the following Dirichlet BVPs:

$$\begin{cases} \mathcal{L}_\varepsilon[e_r](x) = O(\Delta\tau^3), \\ e_r(0) = 0, \quad e_r(L) = 0. \end{cases} \tag{37}$$

The boundedness of inverse operator given in (30) helps us to show that

$$\|e_r\|_\infty \leqslant \|\mathcal{L}_\varepsilon^{-1}\|_\infty O(\Delta\tau^3).$$

Now, the desired result is proved. □

Let us combine the consistency and the stability presented semi-discretized BVP (28)–(29). In the following result, we derive an upper bound for the global error estimate (GEE) defined by:

$$E_r(x) \coloneqq \psi(x, \tau_r) - \Psi_r(x), \quad r \leqslant \frac{T}{\Delta\tau}.$$

It should be stressed that all LEE up to time level contributes to the GEE at time instant τ_r.

Lemma 3.4. (GEE) *Under the assumption of Lemma* 3.3, *the GEE in the time direction satisfies*

$$\|E_r\|_\infty = O(\Delta\tau^2), \quad \forall r\Delta\tau \leqslant T. \tag{38}$$

Proof. After summing the LEE given via Relation (31) in Lemma 3.3 over $s = 1, 2, \ldots, r$, one obtains

$$\begin{aligned} \|E_r\|_\infty &= \left\| \sum_{s=1}^{r} e_s \right\|_\infty \quad (r\Delta\tau \leqslant T) \\ &\leqslant \|e_1\|_\infty + \|e_2\|_\infty + \ldots + \|e_r\|_\infty \\ &\leqslant r(C_1\Delta\tau^3) = C_1(r\Delta\tau)\Delta\tau^2 \\ &\leqslant C_1 T\Delta\tau^2 = O(\Delta\tau^2), \end{aligned}$$

where the constant C_1 is not dependent on $\Delta\tau$. □

The previous Lemma indicates that the presented time discretized approach is uniformly convergent with order 2.

Remark 3.5. Similar lemmas and results can be proved for the semi-discretized approach (22) via the Rothe method. In this case, the LEE and GEE satisfy $||e_r||_\infty = O(\Delta\tau^2)$ and $||E_r||_\infty = O(\Delta\tau)$ for all $r\Delta\tau \leqslant T$, respectively. Thus, the order of (uniform) convergence is one as expected.

4 Two hybrid approaches

In the previous parts, the Rothe and Taylor approaches are used to discretize the parabolic CDR equation (1) with respect to time. These two discretized time equations are given by Relations (22) as well as (26)–(27). Our goal is here to solve these initial BVPs with respect to the spatial variable x.

In both methods and at each time step τ_r, the solutions $w_r(x)$ are approximated as a combination of SDPs (19). Supposedly, we have $\mathcal{W}_{r-1,M}(x)$ as the Delannoy approximation to $w_{r-1}(x)$ at time level τ_{r-1}. Note that for $r = 1$, we utilize the initial condition $g(x)$ for $w_0(x)$. Proceeding in the next time level τ_r, we take the approximate solution $\mathcal{W}_{r,M}(x)$ for $r = 1, 2, \ldots, R$ as:

$$\mathcal{W}_{r,M}(x) = \sum_{m=0}^{M} p_m^r \mathbb{D}_m^\star(x), \quad x \in \Omega_x. \tag{39}$$

In both Rothe-Delannoy and Taylor-Delannoy techniques presented in the following, we seek the unknowns p_m^r, $m = 0, 1, \ldots, M$. By introducing

$$P_M^r = [p_0^r \quad p_1^r \quad \ldots \quad p_M^r]^t, \quad \boldsymbol{D}_M(x) = [\mathbb{D}_0^\star(x) \quad \mathbb{D}_1^\star(x) \quad \ldots \quad \mathbb{D}_M^\star(x)],$$

we may express $\mathcal{W}_{r,M}(x)$ as:

$$\mathcal{W}_{r,M}(x) = \boldsymbol{D}_M(x) P_M^r. \tag{40}$$

It is also not a difficult task to show that the vector of SDFs, i.e., $\boldsymbol{D}_M(x)$ can be written as:

$$\boldsymbol{D}_M(x) = \chi_M(x) K_M, \tag{41}$$

where $\chi_M(x)$ as the vector consisting of powers of $(x - L)$ is given by:

$$\chi_M(x) = [1 \quad x - L \quad (x - L)^2 \quad \ldots \quad (x - L)^M],$$

and K_M as a lower-triangular matrix is defined by:

$$K_M = \begin{pmatrix} \binom{0}{0}\binom{0}{0} & \binom{1}{0}\binom{1}{0} & \binom{2}{0}\binom{2}{0} & \cdots & \binom{M-1}{0}\binom{M-1}{0} & \binom{M}{0}\binom{M}{0} \\ 0 & L^{-1}\binom{1}{1}\binom{2}{1} & L^{-1}\binom{2}{1}\binom{3}{1} & \cdots & L^{-1}\binom{M-1}{1}\binom{M}{1} & L^{-1}\binom{M}{1}\binom{M+1}{1} \\ 0 & 0 & L^{-2}\binom{2}{2}\binom{4}{2} & \cdots & L^{-2}\binom{M-1}{2}\binom{M+1}{2} & L^{-2}\binom{M}{2}\binom{M+2}{2} \\ \vdots & \vdots & \ddots & \ddots & \ddots & \vdots \\ 0 & 0 & 0 & \cdots & L^{1-M}\binom{M-1}{M-1}\binom{2M-2}{M-1} & L^{1-M}\binom{M}{M-1}\binom{2M-1}{M-1} \\ 0 & 0 & 0 & \cdots & 0 & L^{-M}\binom{M}{M}\binom{2M}{M} \end{pmatrix}_{(M+1)\times(M+1)}.$$

It can be clearly seen that

$$\det(K_M) = \prod_{j=0}^{M} L^{-j} \binom{j}{j} \binom{2j}{j} = L^{-M(M+1)/2} \prod_{j=1}^{M} \binom{2j}{j},$$

which is non-zero. Therefore, K_M is in an invertible matrix. With the aid of Relation (41), we have

$$\mathcal{W}_{r,M}(x) = \boldsymbol{D}_M(x) P_M^r = \chi_M(x) K_M P_M^r. \tag{42}$$

One can also prove that the derivatives of $\chi_M(x)$ can be written in terms of itself. To be more precise, we have

$$\frac{\mathrm{d}^v}{\mathrm{d}x^v}\chi_M(x) = \chi_M(x)(E_M)^v, \quad E_M = \begin{pmatrix} 0 & 1 & 0 & \dots & 0 \\ 0 & 0 & 2 & \dots & 0 \\ \vdots & \vdots & \ddots & \vdots & \vdots \\ 0 & 0 & 0 & \ddots & M \\ 0 & 0 & 0 & \dots & 0 \end{pmatrix}_{(M+1)\times(M+1)}, \tag{43}$$

for $v = 1, 2$. Indeed, E_M is called the differentiation matrix. A set of collocation points on Ω_x must be given to obtain the numerical solutions of BVPs (22) as well as (26)–(27). Thus, a uniform partitioning of Ω_x in the following form is considered

$$x_\xi = \frac{L\xi}{M}, \quad \xi = 0, 1, \dots, M. \tag{44}$$

In Relation (42), we differentiate twice with regard to the variable x. Utilizing Relation (43) to obtain

$$\begin{cases} \mathcal{W}_{r,M}^{(1)}(x) = \chi_M(x) E_M K_M P_M^r, \\ \mathcal{W}_{r,M}^{(2)}(x) = \chi_M(x)(E_M)^2 K_M P_M^r. \end{cases} \tag{45}$$

The following theorem states the ways that the approximate solutions $\mathcal{W}_{r,M}(x)$, $\frac{\mathrm{d}}{\mathrm{d}x}\mathcal{W}_{r,M}(x)$, and $\frac{\mathrm{d}^2}{\mathrm{d}x^2}\mathcal{W}_{r,M}(x)$ can be written in the matrix forms. We proceed by defining the following vectors:

$$X_M = \begin{pmatrix} \chi_M(x_0) \\ \chi_M(x_1) \\ \vdots \\ \chi_M(x_M) \end{pmatrix}, \quad W_r = \begin{pmatrix} \mathcal{W}_{r,M}(x_0) \\ \mathcal{W}_{r,M}(x_1) \\ \vdots \\ \mathcal{W}_{r,M}(x_M) \end{pmatrix}, \quad W_r^{(1)} = \begin{pmatrix} \mathcal{W}_{r,M}^{(1)}(x_0) \\ \mathcal{W}_{r,M}^{(1)}(x_1) \\ \vdots \\ \mathcal{W}_{r,M}^{(1)}(x_M) \end{pmatrix}, \quad W_r^{(2)} = \begin{pmatrix} \mathcal{W}_{r,M}^{(2)}(x_0) \\ \mathcal{W}_{r,M}^{(2)}(x_1) \\ \vdots \\ \mathcal{W}_{r,M}^{(2)}(x_M) \end{pmatrix}. \tag{46}$$

Theorem 4.1. *For $r = 1, 2, \dots, R$, the matrix representations of $\frac{\mathrm{d}^v}{\mathrm{d}x^v}\mathcal{W}_{r,M}(x)$ at the set of collocation points* (44) *are given by*:

$$W_r = X_M K_M P_M^r, \tag{47}$$

$$W_r^{(1)} = X_M E_M K_M P_M^r, \tag{48}$$

$$W_r^{(2)} = X_M (E_M)^2 K_M P_M^r. \tag{49}$$

Proof. The proof is straightforward by placing the points (44) into Relations (40)–(45) followed by utilizing the defined vectors (46). □

4.1 Rothe-Delannoy method

We now turn to Relation (22) and write it in a compact form by letting its corresponding coefficients as:

$$\sigma_{2,r}(x) \coloneqq -\varepsilon\Delta\tau, \quad \sigma_{1,r}(x) \coloneqq -\mu\Delta\tau B_r(x), \quad \sigma_{0,r}(x) \coloneqq 1 + \Delta\tau A_r(x),$$
$$H_r(x) \coloneqq \Delta\tau h_r(x) + w_{r-1}(x).$$

Afterward, we substitute the set of collocation points (44) into the resulting equations to arrive at:

$$\sigma_{2,r}(x_\xi)w_r''(x_\xi) + \sigma_{1,r}(x_\xi)w_r'(x_\xi) + \sigma_{0,r}(x_\xi)w_r(x_\xi) = H_r(x_\xi), \tag{50}$$

for $r = 1, 2, \ldots, R$. In the matrix notation, we express the latter equations compactly as:

$$\Sigma_{2,r}W_r^{(2)} + \Sigma_{1,r}W_r^{(1)} + \Sigma_{0,r}W_r = \boldsymbol{H}_r, \quad r = 1, 2, \ldots, R, \tag{51}$$

where the vector $\boldsymbol{H}_r$ and coefficient matrices $\Sigma_{j,r}$, $j = 0, 1, 2$ are given by:

$$\boldsymbol{H}_r = \begin{pmatrix} H_r(x_0) \\ H_r(x_1) \\ \vdots \\ H_r(x_M) \end{pmatrix}_{(M+1)\times 1}, \quad \Sigma_{j,r} = \begin{pmatrix} \sigma_{j,r}(x_0) & 0 & \ldots & 0 \\ 0 & \sigma_{j,r}(x_1) & \ldots & 0 \\ \vdots & \vdots & \ddots & \vdots \\ 0 & 0 & \ldots & \sigma_{j,r}(x_M) \end{pmatrix}_{(M+1)\times(M+1)}.$$

Now, for $r = 1, 2, \ldots, R$, we obtain the fundamental matrix equation by placing Relation (47) into the former equation (51) as:

$$Y_r P_M^r = \boldsymbol{H}_r, \quad [Y_r; \boldsymbol{H}_r], \tag{52}$$

where

$$Y_r \coloneqq \{\Sigma_{2,r}X_M(E_M)^2 + \Sigma_{1,r}X_M E_M + \Sigma_{0,r}X_M\}K_M.$$

4.2 Taylor-Delannoy method

Similar to the latter Rothe-Delannoy approach, we consider Relation (26) and inserting the set of collocation points (44) into it to obtain

$$\sigma_{2,r-1}(x_\xi)w_r''(x_\xi) + \sigma_{1,r-1}(x_\xi)w_r'(x_\xi) + \sigma_{0,r-1}(x_\xi)w_r(x_\xi) = H_{r-1}(x_\xi), \tag{53}$$

for $r = 1, 2, \ldots, R$. We next introduce the vector $\boldsymbol{H}_{r-1}$ and the coefficient matrices $\Sigma_{j,r-1}$, $j = 0, 1, 2$ as:

$$\boldsymbol{H}_{r-1} = \begin{pmatrix} H_{r-1}(x_0) \\ H_{r-1}(x_1) \\ \vdots \\ H_{r-1}(x_M) \end{pmatrix}, \quad \Sigma_{j,r-1} = \begin{pmatrix} \sigma_{j,r-1}(x_0) & 0 & \ldots & 0 \\ 0 & \sigma_{j,r-1}(x_1) & \ldots & 0 \\ \vdots & \vdots & \ddots & \vdots \\ 0 & 0 & \ldots & \sigma_{j,r-1}(x_M) \end{pmatrix}.$$

Therefore, we are now able to rewrite the system of equations in a compact representation form as:

$$\Sigma_{2,r-1}W_r^{(2)} + \Sigma_{1,r-1}W_r^{(1)} + \Sigma_{0,r-1}W_r = \boldsymbol{H}_{r-1}, \quad r = 1, 2, \ldots, R. \tag{54}$$

By setting

$$Y_{r-1} \coloneqq \{\Sigma_{2,r-1}X_M(E_M)^2 + \Sigma_{1,r-1}X_M E_M + \Sigma_{0,r-1}X_M\}K_M,$$

and putting Relations (47) into the corresponding equation (54), we arrive at related fundamental matrix equation:

$$Y_{r-1}P_M^r = \boldsymbol{H}_{r-1}, \quad [Y_{r-1}; \boldsymbol{H}_{r-1}]. \tag{55}$$

4.3 Matrix expressions of boundary conditions

The fundamental matrix equations in both Rothe and Taylor-Delannoy techniques are obtained in the last parts. The implementations of boundary conditions have so far been left undone. We need to incorporate the related boundary conditions (22) and (27) into it in both approaches. We consider the relation (40) and let $x \to 0, L$ in order to implement the boundary conditions. Thus, we obtain

$$\widehat{Y}_r^0 P_M^r = a_0^r, \quad \widehat{Y}_r^0 \coloneqq \chi_M(0)K_M,$$
$$\widehat{Y}_r^L P_M^r = a_L^r, \quad \widehat{Y}_r^L \coloneqq \chi_M(L)K_M.$$

Or equivalently, we obtain two rows $[\widehat{Y}_r^0; a_0^r]$ and $[\widehat{Y}_r^L; a_L^r]$ in each time step τ_r. We now replace two rows of the fundamental matrix equations $[Y_r; \boldsymbol{H}_r]$ and $[Y_{r-1}; \boldsymbol{H}_{r-1}]$ in (52) and (55), respectively, by the two above new rows. We finally obtain the modified matrix equations denoted by $[\widehat{Y}_r; \widehat{\boldsymbol{H}}_r]$ and $[\widehat{Y}_{r-1}; \widehat{\boldsymbol{H}}_{r-1}]$. In each case, by solving the modified equation, we obtain the Delannoy coefficients $p_0^r, p_1^r, \ldots, p_M^r$ in each time level.

4.4 Convergence analysis of the hybrid schemes

Let us investigate the convergence analysis of two proposed hybrid techniques, namely, the Talyor/Rothe-Delannoy approaches. In this respect, we define the error function:

$$E_{r,M}(x) \coloneqq w(x, \tau_r) - \mathcal{W}_{r,M}(x), \quad x \in \Omega_x. \tag{56}$$

The next theorem establishes that the method is uniformly convergent with respect to both space and time variables.

Theorem 4.2. *Suppose that* $w(x, \tau) \in C^{(2,3)}(\Omega)$ *is the exact solution of* (1). *Also, suppose that the solution* $w_r(x)$ *of* (26) *or* (28) *satisfies the hypotheses of Theorem* 2.6. *Then, the following estimate for the (global) error* $E_{r,M}(x)$ *holds*

$$||E_{r,M}||_\infty = O\left(\Delta\tau^2 + \frac{1}{\sqrt{M}}\right), \quad r\Delta\tau \leqslant T.$$

Proof. By applying the triangle inequality, we have

$$||E_{r,M}||_\infty \leqslant ||w(x, \tau_r) - w_r(x)||_\infty + ||w_r(x) - \mathcal{W}_{r,M}(x)||_\infty.$$

We use the estimate (38) proved in Lemma 3.4 for the first term in above. For the second term, it is sufficient to use the estimate (20) given in Theorem 2.7 with $w_r(x)$ instead of $f(x)$. □

In view of Remark (3.5) and under condition $w(x, \tau) \in C^{(2,2)}(\Omega)$ is the exact solution of (1), we can similarly prove that the Rothe-Delannoy collocation technique is uniformly convergent of order $||E_{r,M}||_\infty = O\left(\Delta\tau + \frac{1}{\sqrt{M}}\right)$ for all $r\Delta\tau \leqslant T$.

5 Graphical and implementation results

In this part, a set of numerical simulations is performed to demonstrate the accuracy of the proposed Rothe/Taylor-Delannoy collocation matrix techniques and support the theoretical findings. For validation of the obtained results, a comparison will be drawn between the numerical outcomes of some available

computational procedures. The experiments were conducted on an ASUS laptop computer with 16 GB RAM and with 2.2 GHz Intel Core i7 CPU. We used Matlab software version 2021a.

Test example 5.1. As an academic test case, we first set the related coefficients and non-homogeneous term in (1) as given by [7]:

$$B(x,\tau) = -(1+e^{x}), \quad A(x,\tau) = 1 + x^{4}|x|, \quad h(x,\tau) = 10(x^{2}-x^{4})e^{\tau^{2}}.$$

The initial and boundary conditions are given for $L = 1$ as:

$$g(x) = x^{3}(1-x^{3}), \quad a_{0}(\tau) = 0, \quad a_{L}(\tau) = 0.$$

Test example 5.2. In the second test problem, we take the following coefficients as [7–9]:

$$B(x,\tau) = -(\tau^{2}+1+x-x^{2}), \quad A(x,\tau) = 1 + 5x\tau, \quad h(x,\tau) = (e^{\tau}-1)x(1-x).$$

For $L = 1$, we have the next initial and boundary conditions:

$$g(x) = 0, \quad a_{0}(\tau) = 0, \quad a_{L}(\tau) = 0.$$

No exact solutions are given for these two test cases. Thus, we consider the residual error functions (REFs) defined at time level τ_r related to the Rothe and Taylor approaches given by:

$$\begin{cases} \mathbb{R}^{Rot}_{r,M}(x) \coloneqq |\sigma_{2,r}(x)\mathcal{W}^{(2)}_{r,M}(x) + \sigma_{1,r}(x)\mathcal{W}^{(1)}_{r,M}(x) + \sigma_{0,r}(x)\mathcal{W}_{r,M}(x) - H_{r}(x)|, \\ \mathbb{R}^{Tay}_{r,M}(x) \coloneqq |\sigma_{2,r-1}(x)\mathcal{W}^{(2)}_{r,M}(x) + \sigma_{1,r-1}(x)\mathcal{W}^{(1)}_{r,M}(x) + \sigma_{0,r-1}(x)\mathcal{W}_{r,M}(x) - H_{r-1}(x)|, \end{cases} \quad x \in \Omega_{x}, \tag{57}$$

for $r = 1,\dots,R$. Note that the coefficients $\sigma_{i,s}(x)$, $i = 0,1,2$, and $s = r, r-1$ are defined in (50) and (26), respectively. Furthermore, the norms of REFs in the L_∞ and L_2 at the final time step τ_R are

$$\mathbb{R}_{\infty} \equiv \mathbb{R}_{\infty}(R,M) \coloneqq \max_{x\in\Omega_{x}} \mathbb{R}^{\mathrm{Rot/Tay}}_{R,M}(x), \quad \mathbb{R}_{2} \equiv \mathbb{R}_{2}(R,M) \coloneqq \|\mathbb{R}^{\mathrm{Rot/Tay}}_{R,M}(x)\|_{2}.$$

The following formulae are further utilized to calculate the obtained order of convergence (OC) related to both numerical techniques (by fixing R or M) given by:

$$\mathrm{OC}\,\tau_{d} \coloneqq \log_{2}\left(\frac{\mathbb{R}_{d}(R,M)}{\mathbb{R}_{d}(2R,M)}\right), \quad \mathrm{OC}\,x_{d} \coloneqq \log_{2}\left(\frac{\mathbb{R}_{d}(R,M)}{\mathbb{R}_{d}(R,2M)}\right), \quad d = 2,\infty. \tag{58}$$

5.1 Rothe-Delannoy approach

We first consider the parameters $\varepsilon, \mu = 0.1$. Using $M = 10$ and $\Delta\tau = 0.1$, the approximate solutions are obtained in the following forms at the time step $\tau = T$ for Examples 5.1 and 5.2, respectively,

$$\begin{aligned} \mathcal{W}_{10,10}(x) &= -3.00485(x-1)x^{10} - 20.3634(x-1)^{9} - 61.4892(x-1)^{8} - 105.775(x-1)^{7} - 108.697(x-1)^{6} \\ &\quad - 57.5927(x-1)^{5} - 5.86718(x-1)^{4} - 4.79809(x-1)^{3} - 20.5385(x-1)^{2} - 11.0679(x-1), \\ \mathcal{W}_{10,10}(x) &= -0.183164(x-1)x^{10} - 0.956985(x-1)^{9} - 2.24824(x-1)^{8} - 3.34094(x-1)^{7} - 3.33467(x-1)^{6} \\ &\quad - 2.38496(x-1)^{5} - 1.32992(x-1)^{4} - 0.409884(x-1)^{3} - 0.255003(x-1)^{2} - 0.258238(x-1). \end{aligned}$$

The profile of approximate solutions in the whole domain $(x,\tau) \in [0,1]\times[0,1]$ is visualized in Figures 1 and 2. The related REFs obtained via relation (57) are also depicted along with these plots. We emphasize that we can obtain more accuracy by increasing M or by decreasing $\Delta\tau$. To confirm this fact, we take $M = 20$ and $\Delta\tau = 0.01$ in the next experiment. Figure 3 shows the achieved REFs obtained via these aforesaid parameters related to both numerical examples.

It can be realized that the theoretical OC of the Rothe-Delannoy collocation approach is $O(\Delta\tau)$ in time and has an exponential behavior as proved in Theorem 2.6. To justify these facts, we calculate the OC via (58) in the

next results using $\varepsilon, \mu = 10^{-2}$. The results using fixed $M = 4$ and different values of $\Delta\tau = 2^{-s}$, $s = 1, 2, 3, 4$ are tabulated in Tables 1 and 2 for Examples 5.1 and 5.2, respectively. Similarly, the outcomes by fixing $\Delta\tau = 1/16$ and utilizing various $M = 2^s$, $s = 1, 2, 3, 4$ are reported in Tables 1 and 2. As one expected, the first-order accuracy with respect to time and a high-order accuracy in space are observable from the results shown in this table.

A comparison with respect to L_∞ error norm has been done in Table 3 to validate our results obtained via the Rothe-Delannoy technique. In this respect, we use $(\Delta\tau, M) = (\frac{1}{32}, 16)$ and diverse values of (ε, μ) are utilized. Also, the outcomes of an existing numerical method, i.e., the moving mesh-adaptive algorithm (MMAA) [7], are further mentioned in Table 3 with parameters $(\Delta\tau, M) = (\frac{1}{32}, 128), (\frac{1}{256}, 1024)$. In [7], M denotes the number of spatial grid points. Clearly, our algorithm with a small number of M and a higher value of $\Delta\tau$ is more accurate than MMAA. Similar results using a smaller set of (ε, μ) but for $(\Delta\tau, M) = (\frac{1}{16}, 10)$ are presented in Table 4 related to Example 5.2. Here, we compared our results with the method developed in [8] besides the MMAA with parameters $(\Delta\tau, M) = (\frac{1}{128}, 512)$. In this approach, the Richardson extrapolation procedure is used for the time stepping, while a combined monotone finite difference operator is designed for the space variable using a piecewise uniform Shishkin mesh. It is evident the proposed numerical technique produces higher accurate results against the methods developed in [7] and [8].

Finally, in the first part and in the Rothe-Delannoy technique, we utilize two small values of $\varepsilon = 10^{-8}$ and $\mu = 10^{-6}$. In this case, we use $\Delta\tau = 1/32$ and $M = 14$. The graphical representations of the approximate solution together with the related REFs are shown in Figures 4 and 5 associated with Examples 5.1 and 5.2, respectively.

5.2 Taylor-Delannoy approach

Analog to the Rothe-Delannoy method, we first take the parameters $\varepsilon, \mu = 0.1$. The approximate solutions for Examples 5.1 and 5.2 at time step $\tau = T$ utilizing $M = 10$ and $\Delta\tau = 0.1$ take the following forms, respectively,

$$\begin{aligned}\mathcal{W}_{10,10}(x) &= -2.83681(x-1)x^{10} - 19.2256(x-1)x^9 - 58.179(x-1)^8 - 100.26(x-1)^7 - 103.057(x-1)^6 \\ &\quad - 54.2433(x-1)^5 - 4.97596(x-1)^4 - 4.56666(x-1)^3 - 20.0702(x-1.0)^2 - 10.8142(x-1), \\ \mathcal{W}_{10,10}(x) &= 0.185724(x-1)^10 + 0.978579(x-1)^9 + 2.29962(x-1)^8 + 3.39476(x-1)^7 + 3.36605(x-1)^6 \\ &\quad + 2.39168(x-1)^5 + 1.31676(x-1)^4 + 0.398006(x-1)^3 + 0.251874(x-1)^2 + 0.257017(x-1).\end{aligned}$$

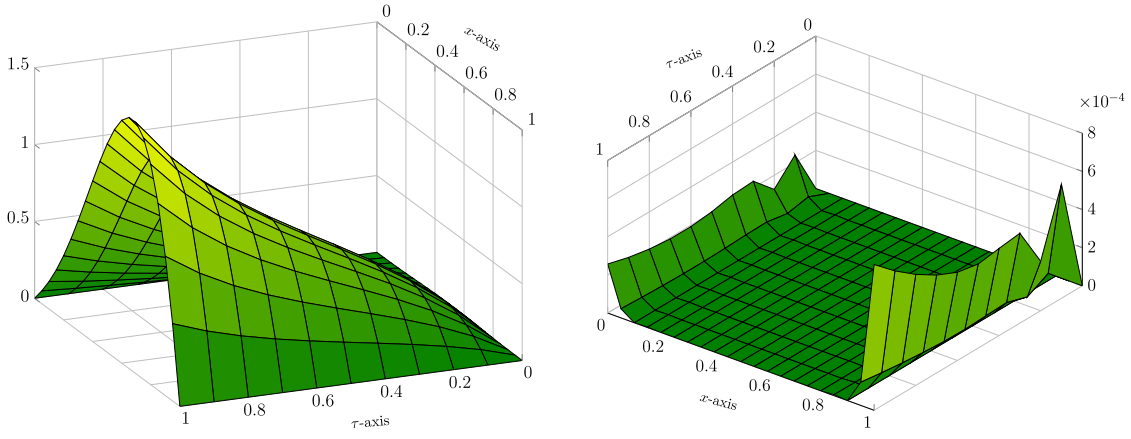

Figure 1: Approximate solution obtained via the Rothe-Delannoy approach (left) and the REFs (right) in Example 5.1 with $\varepsilon, \mu = 10^{-1}$, $\Delta\tau = 0.1$, $T = 1$, and $M = 10$.

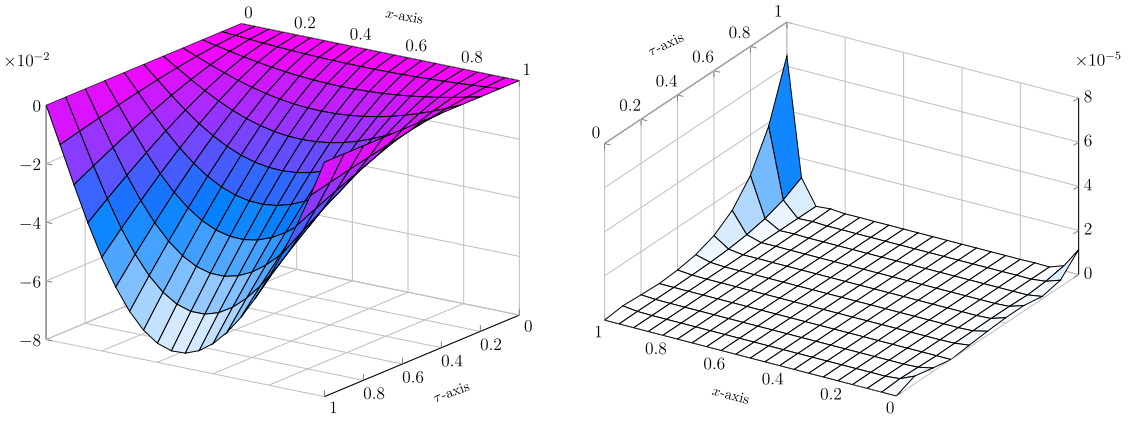

Figure 2: Approximate solution obtained via the Rothe-Delannoy approach (left) and the REFs (right) in Example 5.2 with $\varepsilon, \mu = 10^{-1}$, $\Delta\tau = 0.1$, $T = 1$, and $M = 10$.

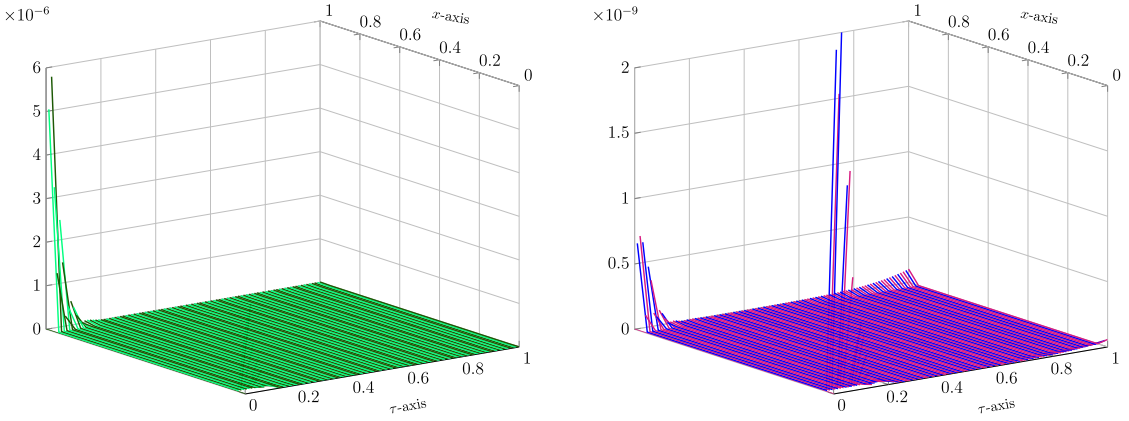

Figure 3: Visualization of REFs in the Rothe-Delannoy approach at different time instants τ_r, $r = 1, 2, \ldots, 100$ in Example 5.1 (left) and Example 5.2 (right) for $\Delta\tau = 0.01$, $M = 20$, $\varepsilon, \mu = 10^{-1}$, and $T = 1$.

Table 1: $\mathbb{R}_2$ and $\mathbb{R}_\infty$ error norms the achieved OC in the Rothe-Delannoy approach in Example 5.1 with a fixed $M = 4$, $\Delta\tau = 1/32$, $\varepsilon, \mu = 10^{-2}$, $T = 1$, and various $\Delta\tau$, M

	$M = 4$					$\Delta\tau = 1/16$			
$\Delta\tau$	$\mathbb{R}_2$	$\mathrm{OC}\,\tau_2$	$\mathbb{R}_\infty$	$\mathrm{OC}\,\tau_\infty$	M	$\mathbb{R}_2$	OCx_2	$\mathbb{R}_\infty$	OCx_∞
$\frac{1}{2}$	4.1642×10^{-2}	—	2.0863×10^{-1}	—	2	6.6509×10^{-2}	—	1.7112×10^{-1}	—
$\frac{1}{4}$	1.9564×10^{-2}	1.0898	9.9282×10^{-2}	1.0713	4	4.6445×10^{-3}	3.8400	2.3750×10^{-2}	2.8490
$\frac{1}{8}$	9.4531×10^{-3}	1.0494	4.8228×10^{-2}	1.0417	8	3.6127×10^{-4}	3.6844	7.3733×10^{-3}	1.6875
$\frac{1}{16}$	4.6445×10^{-3}	1.0253	2.3750×10^{-2}	1.0220	16	4.8071×10^{-6}	6.2318	2.1273×10^{-4}	5.1152

The graphical representation of approximate solutions in the whole domain $(x, \tau) \in [0, 1] \times [0, 1]$ is shown in Figure 6. To obtain a higher accuracy, we increase the number of basis M or decrease $\Delta\tau$. For Example 5.1 and in Table 5, we first fix $M = 20$ and vary $\Delta\tau$ to see how the $\mathrm{OC}\,\tau_d$ in time are behaved. Here, we utilize $\varepsilon, \mu = 10^{-2}$ in the computations. Hence, we fix $\Delta\tau = 1/16$ and vary $M = 2, 4, 8, 16$. The results of OCx_d are reported in the second part of Table 5 for $d = 2, \infty$. Clearly, the second-order accuracy in τ and a higher-order accuracy in x are

Table 2: $\mathbb{R}_2$ and $\mathbb{R}_\infty$ error norms the achieved OC in the Rothe-Delannoy approach in Example 5.2 with a fixed $M = 4$, $\Delta\tau = 1/32$, $\varepsilon, \mu = 10^{-2}$, $T = 1$, and various $\Delta\tau$, M

	$M = 4$					$\Delta\tau = 1/16$			
$\Delta\tau$	$\mathbb{R}_2$	$\mathbf{OC}\tau_2$	$\mathbb{R}_\infty$	$\mathbf{OC}\tau_\infty$	M	$\mathbb{R}_2$	$\mathbf{OCx}_2$	$\mathbb{R}_\infty$	$\mathbf{OCx}_\infty$
$\frac{1}{2}$	1.5722×10^{-3}	—	1.7828×10^{-2}	—	2	2.0157×10^{-3}	—	5.0315×10^{-3}	—
$\frac{1}{4}$	7.1666×10^{-4}	1.1334	7.9780×10^{-3}	1.1601	4	1.6405×10^{-4}	3.6190	1.7824×10^{-3}	1.4972
$\frac{1}{8}$	3.3865×10^{-4}	1.0815	3.7150×10^{-3}	1.1027	8	4.3763×10^{-5}	1.9064	8.5134×10^{-4}	1.0660
$\frac{1}{16}$	1.6405×10^{-4}	1.0456	1.7824×10^{-3}	1.0595	16	3.7332×10^{-7}	6.8732	1.6209×10^{-5}	5.7148

Table 3: Comparisons of error norms in Rothe-Delannoy approach in Example 5.1 with $M = 16$, $\Delta\tau = 1/32$, and various ε, μ

	Present: $(\Delta\tau, M) = (\frac{1}{32}, 16)$		**MMAA [7] (Maximum errors)**	
(ε, μ)	$\mathbb{R}_\infty$	$\mathbb{R}_2$	$(\Delta\tau, M) = (\frac{1}{32}, 128)$	$(\Delta\tau, M) = (\frac{1}{256}, 1024)$
$(10^{-2}, 10^{-4})$	1.3431×10^{-4}	3.1523×10^{-6}	1.1005×10^{-2}	1.3370×10^{-3}
$(10^{-3}, 10^{-4})$	4.2173×10^{-4}	1.1160×10^{-5}	1.1976×10^{-2}	1.4690×10^{-3}
$(10^{-4}, 10^{-4})$	6.3133×10^{-5}	1.0522×10^{-6}	1.1985×10^{-2}	1.4780×10^{-3}
$(10^{-5}, 10^{-4})$	1.6381×10^{-4}	3.5362×10^{-6}	1.2011×10^{-2}	1.4850×10^{-3}
$(10^{-5}, 10^{-6})$	8.9921×10^{-6}	2.4677×10^{-7}	1.1856×10^{-2}	1.4840×10^{-3}
$(10^{-6}, 10^{-6})$	6.6773×10^{-7}	2.0028×10^{-8}	1.1922×10^{-2}	1.4790×10^{-3}
$(10^{-7}, 10^{-6})$	1.6409×10^{-6}	3.6331×10^{-8}	1.2279×10^{-2}	1.4720×10^{-3}

Table 4: Comparisons of error norms in Rothe-Delannoy approach in Example 5.2 with $M = 10$, $\Delta\tau = 1/16$, and various ε, μ

	Present: $(\Delta\tau, M) = (\frac{1}{16}, 10)$		$(\Delta\tau, M) = (\frac{1}{128}, 512)$	
(ε, μ)	$\mathbb{R}_\infty$	$\mathbb{R}_2$	**MMAA [7]**	**Richardson [8]**
$(10^{-6}, 10^{-7})$	1.5753×10^{-7}	5.8572×10^{-9}	1.2824×10^{-4}	6.6241×10^{-7}
$(10^{-7}, 10^{-7})$	2.2132×10^{-8}	7.0771×10^{-10}	1.2853×10^{-4}	6.6241×10^{-7}
$(10^{-8}, 10^{-7})$	8.5904×10^{-9}	2.6963×10^{-10}	1.2781×10^{-4}	6.6241×10^{-7}
$(10^{-9}, 10^{-7})$	7.2362×10^{-9}	2.4376×10^{-10}	1.2804×10^{-4}	6.6241×10^{-7}

obtainable in the Taylor-Delannoy series method. Similar results for the second Example 5.2 are presented in Table 6 but for different fixed values of $M = 10$ and $\Delta\tau = 1/320$

Similar to the Rothe-Delannoy method, some comparisons are made between our numerical results and the outcomes of the MMAA [7] in Table 7. In these experiments, we have used $M = 16$, $\Delta\tau = 1/32$, and various small values of ε and μ are considered. In contrast, the values $M = 256, 512$ as the number of spatial grid points and $\Delta\tau = 1/64, 1/128$ were used in the MMAA procedure. Needless to say, our results using a larger time step (and with a smaller number of bases) are more accurate in comparison with the outcomes of MMAA.

Ultimately, we consider two small values of $(\varepsilon, \mu) = (10^{-8}, 10^{-6})$. For $\Delta\tau = 1/32$ and $M = 12$, the approximate solutions at the final time $\tau = T$ is given by:

$$\begin{aligned}\mathcal{W}_{1,32}(x) = {} & 28.2824(x-1)^{12} + 176.975(x-1)^{11} + 471.382(x-1)^{10} + 668.581(x-1)^{9} \\ & + 479.111(x-1)^{8} + 43.4217(x-1.0)^{7} - 196.896(x-1)^{6} - 109.513(x-1)^{5} \\ & + 35.4617(x-1)^{4} + 35.5468(x-1)^{3} - 17.2626(x-1)^{2} - 14.932(x-1),\end{aligned}$$

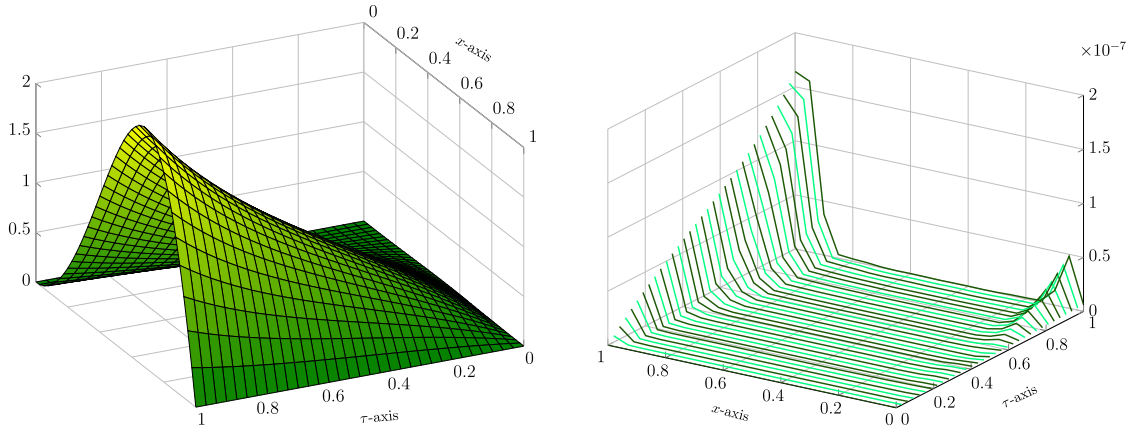

Figure 4: Visualization of approximate solution (right) and the REFs (left) in the Rothe-Delannoy approach at different time instants τ_r, $r = 1, 2, \ldots, 32$ in Example 5.1 for $\Delta\tau = 1/32$, $M = 14$, $\varepsilon = 10^{-8}$, $\mu = 10^{-6}$, and $T = 1$.

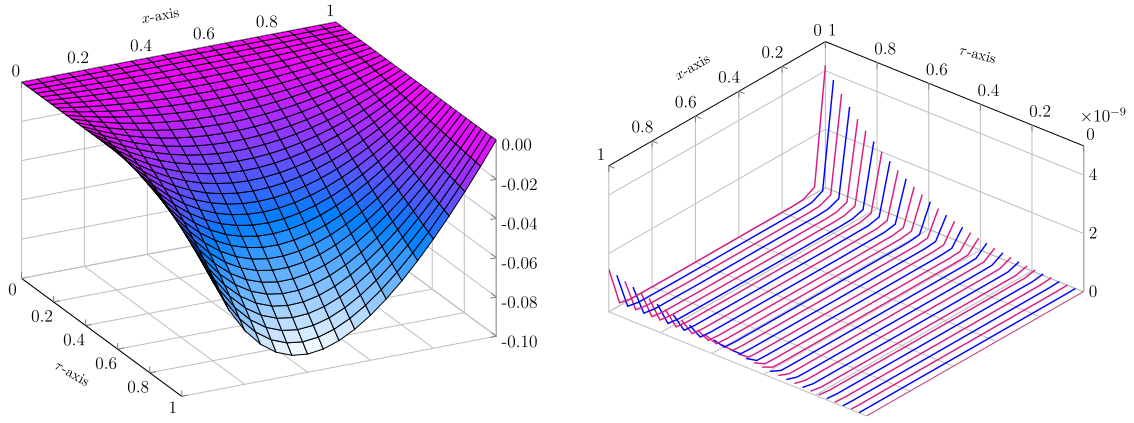

Figure 5: Visualization of approximate solution (right) and the REFs (left) in the Rothe-Delannoy approach at different time instants τ_r, $r = 1, 2, \ldots, 32$ in Example 5.2 for $\Delta\tau = 1/32$, $M = 14$, $\varepsilon = 10^{-8}$, $\mu = 10^{-6}$, and $T = 1$.

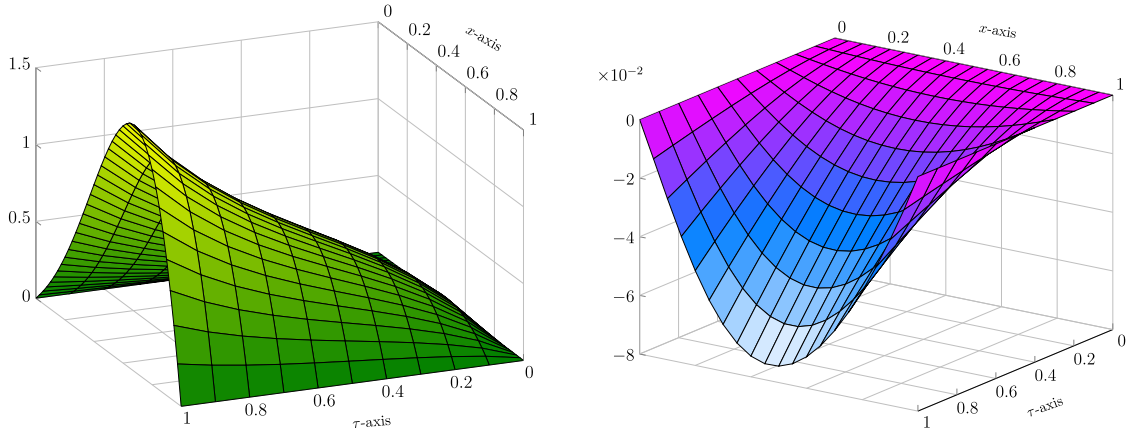

Figure 6: Approximate solutions obtained via the Taylor-Delannoy approach for Example 5.1 (left) and Example 5.2 (right) with $\varepsilon, \mu = 10^{-1}$, $\Delta\tau = 0.1$, $T = 1$, and $M = 10$.

Table 5: $\mathbb{R}_2$ and $\mathbb{R}_\infty$ error norms the achieved OC in the Taylor-Delannoy approach in Example 5.1 with a fixed $M = 20$, $\Delta\tau = 1/16$, $\varepsilon, \mu = 10^{-2}$, $T = 1$, and various $\Delta\tau$, M

	$M = 20$					$\Delta\tau = 1/16$			
$\Delta\tau$	$\mathbb{R}_2$	$\mathbf{OC}\tau_2$	$\mathbb{R}_\infty$	$\mathbf{OC}\tau_\infty$	M	$\mathbb{R}_2$	$\mathbf{OCx}_2$	$\mathbb{R}_\infty$	$\mathbf{OCx}_\infty$
$\frac{1}{2}$	7.6855×10^{-6}	—	4.0077×10^{-4}	—	2	1.2547×10^{-1}	—	3.2306×10^{-1}	—
$\frac{1}{4}$	9.3964×10^{-6}	−0.2900	4.0761×10^{-4}	−0.0244	4	8.6965×10^{-3}	3.8507	4.4586×10^{-2}	2.8571
$\frac{1}{8}$	2.8447×10^{-6}	1.7238	1.4570×10^{-4}	1.4842	8	6.9113×10^{-4}	3.6534	1.4085×10^{-2}	1.6624
$\frac{1}{16}$	6.8003×10^{-7}	2.0646	3.6922×10^{-5}	1.9804	16	9.9786×10^{-6}	6.1140	4.3118×10^{-4}	5.0297

Table 6: $\mathbb{R}_2$ and $\mathbb{R}_\infty$ error norms the achieved OC in the Taylor-Delannoy approach in Example 5.2 with a fixed $M = 10$, $\Delta\tau = 1/320$, $\varepsilon, \mu = 10^{-2}$, $T = 1$, and various $\Delta\tau$, M

	$M = 10$					$\Delta\tau = 1/320$			
$\Delta\tau$	$\mathbb{R}_2$	$\mathbf{OC}\tau_2$	$\mathbb{R}_\infty$	$\mathbf{OC}\tau_\infty$	M	$\mathbb{R}_2$	$\mathbf{OCx}_2$	$\mathbb{R}_\infty$	$\mathbf{OCx}_\infty$
$\frac{1}{2}$	1.3091×10^{-2}	—	6.4420×10^{-2}	—	2	1.9939×10^{-4}	—	4.9898×10^{-4}	—
$\frac{1}{4}$	2.9828×10^{-3}	2.1339	1.4596×10^{-2}	2.1419	4	1.5828×10^{-5}	3.6550	1.6955×10^{-4}	1.5573
$\frac{1}{8}$	7.3089×10^{-4}	2.0289	3.5652×10^{-3}	2.0336	8	4.3493×10^{-6}	1.8636	8.4488×10^{-5}	1.0049
$\frac{1}{16}$	1.8338×10^{-4}	1.9949	8.8603×10^{-4}	2.0085	16	3.6534×10^{-7}	3.5735	2.2103×10^{-6}	5.2564

for the first Example 5.1 and

$$\begin{aligned}\mathcal{W}_{1,32}(x) = &-0.00318951(x-1)^{12} - 0.0164746(x-1)^{11} - 0.036348(x-1)^{10} - 0.0455024(x-1)^9 \\ &- 0.0320158(x-1)^8 - 0.0179865(x-1.0)^7 + 0.00832472(x-1)^6 - 0.0221956(x-1)^5 \\ &+ 0.0447422(x-1)^4 - 0.069024(x-1)^3 + 0.0900682(x-1)^2 + 0.242765(x-1).\end{aligned}$$

for the second Example 5.2. The snapshots of approximate solutions at all time steps are shown in Figures 7 and 8. The pictorial representations of the related REFs for these two examples further are visualized in Figures 7 and 8 (right panels).

Table 7: Comparisons of error norms in Taylor-Delannoy approach in Example 5.1 with $M = 16$, $\Delta\tau = 1/32$, and various ε, μ

	Present: $(\Delta\tau, M) = (\frac{1}{32}, 16)$		MMAA [7] (Maximum errors)	
(ε, μ)	$\mathbb{R}_\infty$	$\mathbb{R}_2$	$(\Delta\tau, M) = (\frac{1}{64}, 256)$	$(\Delta\tau, M) = (\frac{1}{128}, 512)$
$(10^{-5}, 10^{-6})$	1.7491×10^{-5}	4.7820×10^{-7}	5.886×10^{-3}	2.974×10^{-3}
$(10^{-6}, 10^{-6})$	1.2824×10^{-6}	3.8829×10^{-8}	5.909×10^{-3}	2.961×10^{-3}
$(10^{-7}, 10^{-6})$	3.1737×10^{-6}	7.0724×10^{-8}	5.906×10^{-3}	2.961×10^{-3}
$(10^{-8}, 10^{-6})$	3.3630×10^{-6}	7.4950×10^{-8}	6.008×10^{-3}	2.981×10^{-3}

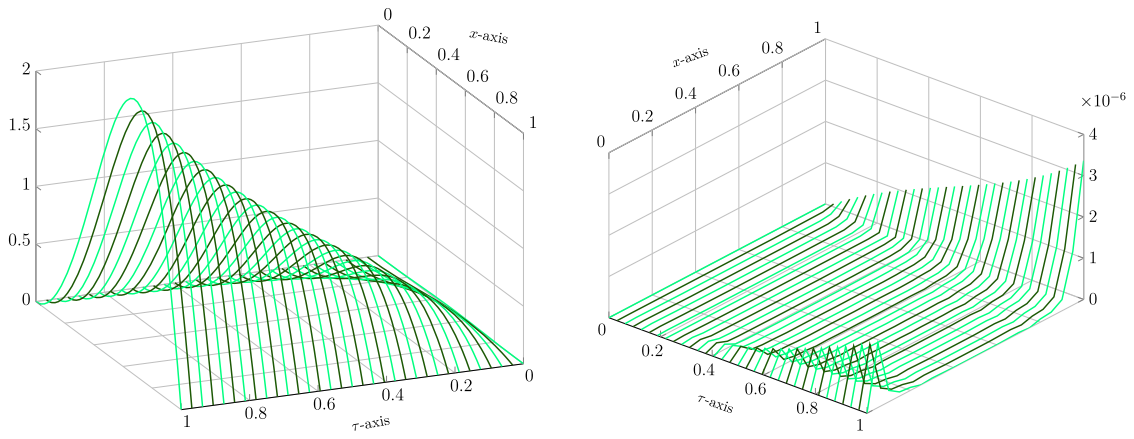

Figure 7: Visualization of approximate solution (left) and the REFs (right) in the Taylor-Delannoy approach at different time instants τ_r, $r = 1, 2, \ldots, 32$ in Example 5.1 for $\Delta\tau = 1/32$, $M = 12$, $\varepsilon = 10^{-8}$, $\mu = 10^{-6}$, and $T = 1$.

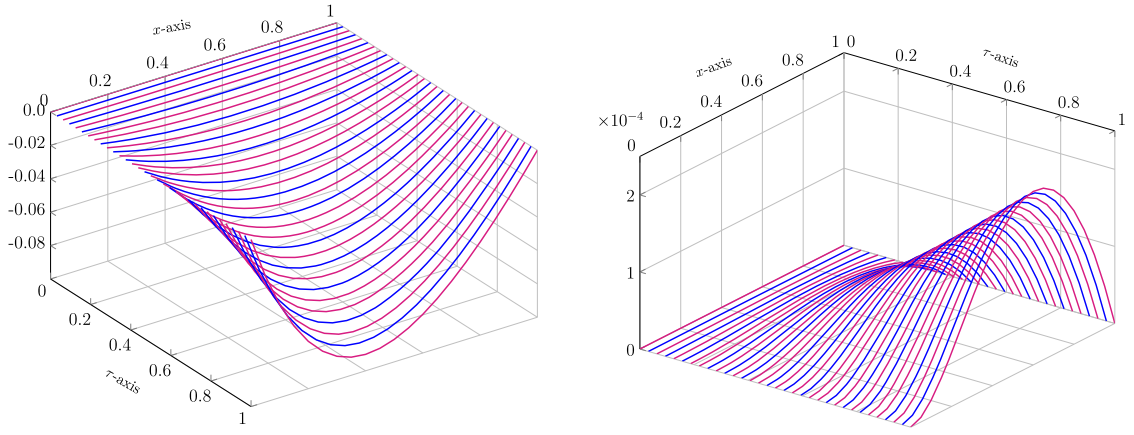

Figure 8: Visualization of approximate solution (left) and the REFs (right) in the Taylor-Delannoy approach at different time instants τ_r, $r = 1, 2, \ldots, 32$ in Example 5.2 for $\Delta\tau = 1/32$, $M = 12$, $\varepsilon = 10^{-8}$, $\mu = 10^{-6}$, and $T = 1$.

6 Conclusion

Two accurate hybrid matrix collocation techniques based on the (novel) Delannoy functions of graph are developed to find an approximate solution to a class of singularly perturbed CDR problems with variable coefficients and two small parameters. For the time-marching algorithms, the first-order Rothe method and the second-order Taylor series formula are utilized to discretize the underlying CDR model problems. We then apply the Delannoy collocation technique to the discretized time equations at each time level. The proposed schemes have been shown to be uniformly convergent of order $O(\Delta\tau^s + 1/M^{\frac{1}{2}})$, $s = 1, 2$. Numerical simulations relied on two academic test cases are presented to demonstrate the first- and second-order accuracy of the proposed hybrid approaches. The presented results show that two new hybrid procedures have better accuracy in comparison with the current numerical methods.

Acknowledgements: Khursheed J. Ansari extends his appreciation to the Deanship of Scientific Research at King Khalid University for funding this work through a large group Research Project under Grant Number RGP2/371/44.

Author contributions: The authors have accepted responsibility for the entire content of this manuscript and approved its submission.

Conflict of interest: The authors state no conflict of interest.

Data availability statement: Data sharing is not applicable to this article as no datasets were generated or analyzed during this study.

References

[1] D. S. Naidu, *Singular perturbations and time scales in control theory and applications: An overview*, Dyn. Contin. Discrete Impuls. Syst. Ser. B Appl. Algorithms **9** (2002), no. 2, 233–278.

[2] S. Polak, C. Den Heiger, W. H. Schilders, and P. Markowich, *Semiconductor device modelling from the numerical point of view*, Int. J. Numer. Methods Eng. **24** (1987), 763–838.

[3] J. J. H. Miller, E. O'riordan, and G. I. Shishkin, *Fitted Numerical Methods for Singular Perturbation Problems: Error Estimates in the Maximum Norm for Linear Problems in One and Two Dimensions*, World Scientific, Singapore, 1996.

[4] J. I. Ramos, *A piecewise-analytical method for singularly perturbed parabolic problems*, Appl. Math. Comput. **161** (2005), 501–512.

[5] M. El-Gamel, *The sinc-Galerkin method for solving singularly perturbed reaction diffusion problem*, Electron. Trans. Numer. Anal. **23** (2006), 129–140.

[6] E. O'Riordan, M. L. Pickett, and G. I. Shishkin, *Parameter-uniform finite difference schemes for singularly perturbed parabolic diffusion-convection-reaction problems*, Math. Comput. **75** (2006), no. 255, 1135–1154.

[7] P. Das and V. Mehrmann, *Numerical solution of singularly perturbed convection–diffusion–reaction problems with two small parameters*, BIT Numer. Math. **56** (2016), no. 1, 51–76.

[8] V. Gupta, M. K. Kadalbajoo, and R. K. Dubey, *A parameter-uniform higher-order finite difference scheme for singularly perturbed time-dependent parabolic problem with two small parameters*, Int. J. Comput. Math. **96** (2019), no. 3, 474–499.

[9] R. Jiwari, S. Sukhveer, and S. Paramjeet, *Local RBF-FD-based mesh-free scheme for singularly perturbed convection–diffusion–reaction models with variable coefficients*, J. Math. **2022** (2022), 3119482.

[10] M. K. Kadalbajoo and A. S. Yadaw, *Parameter uniform finite element method for two parameter singularly perturbed parabolic reaction-diffusion problems*, Int. J. Comput. Methods **9** (2012), no. 4, 1250047.

[11] C. Clavero, J. C. Jorge, and F. Lisbona, *A uniformly convergent scheme on a nonuniform mesh for convection-diffusion parabolic problems*, J. Comput. Appl. Math. **154** (2003), 415–429.

[12] M. K. Kadalbajoo, V. Gupta, and A. Awasthi, *A uniformly convergent B-spline collocation method on a nonuniform mesh for singularly perturbed one dimensional time-dependent linear convection-diffusion problem*, J. Comput. Appl. Math. **220** (2008), 271–289.

[13] K. Mukherjee and S. Natesan, *Richardson extrapolation technique for singularly perturbed parabolic convection-diffusion problems*, Computing **92** (2011), 1–32.

[14] M. M. Woldaregay, W. T. Aniley, and G. F. Duressa, *Novel numerical scheme for singularly perturbed time delay convection-diffusion equation*, Adv. Math. Phys. **2021** (2021), 6641236.

[15] G. T. Lubo and G. F. Duressa, *Redefined cubic B-spine finite element method for the generalized diffusion equation with delay*, Research Math. **9** (2022), no. 1, 2095092.

[16] S. R. Sahu and J. Mohapatra, *Parameter uniform numerical methods for singularly perturbed delay differential equation involving two small parameters*, Int. J. Appl. Comput. Math. **5** (2019), 129.

[17] L. Govindarao and J. Mohapatra, *A second order numerical method for singularly perturbed delay parabolic partial differential equation*, Eng. Comput. **36** (2019), no. 2, 420–444.

[18] M. Izadi, *Streamline diffusion method for treating coupling equations of hyperbolic scalar conservation laws*, Math. Comput. Model. **45** (2007), 201–214.

[19] M. Izadi, *A posteriori error estimates for the coupling equations of scalar conservation laws*, BIT Numer. Math. **49** (2009), no. 4, 697–720.

[20] X. Liu and J. Zhang, *Supercloseness of linear streamline diffusion finite element method on Bakhvalov-type mesh for singularly perturbed convection-diffusion equation in 1D*, Appl. Math. Comput. **430** (2022), 127258.

[21] H. G. Roos, *Error estimates for linear finite elements on Bakhvalov-type meshes*, Appl. Math. **51** (2006), no. 1, 63–72.

[22] J. Zhang and Y. Lv, *Finite element method for singularly perturbed problems with two parameters on a Bakhvalov-type mesh in 2D*, Numer. Algor. **90** (2022), 447–475.

[23] N. T. Negero, *A parameter-uniform efficient numerical scheme for singularly perturbed time-delay parabolic problems with two small parameters*, Partial Differ. Equ. Appl. Math. **7**, (2023), 100518.

[24] H. G. Roos, M. Stynes, and L. Tobiska, *Numerical Methods for Singularly Perturbed Differential Equations*, Springer, Berlin, 1996.

[25] M. Izadi, *Applications of the Newton-Raphson method in a SDFEM for inviscid Burgers equation*, Comput. Methods Differ. Equ. **8** (2020), no. 4, 708–732.
[26] L. Govindarao, J. Mohapatra, and A. Das, *A fourth-order numerical scheme for singularly perturbed delay parabolic problem arising in population dynamics*, J. Appl. Math. Comput. **63** (2020), no. 1, 171–95.
[27] M. Izadi, Ş. Yüzbaşı, and K. J. Ansari, *Application of Vieta-Lucas series to solve a class of multi-pantograph delay differential equations with singularity*, Symmetry **13** (2021), no. 12, 2370.
[28] S. Ahmed, S. Jahan, K. J. Ansari, K. Shah, and T. Abdeljawad, *Wavelets collocation method for singularly perturbed differential-difference equations arising in control system*, Results Appl. Math. **21** (2024), 100415.
[29] M. Izadi and H. M. Srivastava, *An optimized second-order numerical scheme applied to the non-linear Fisheras reaction-diffusion equation*, J. Interdiscip. Math. **25** (2022), no. 2, 471–492.
[30] Ş. Yüzbaşı, and M. Karaçayır, *An approximation technique for solutions of singularly perturbed one-dimensional convection-diffusion problem*, Int. J. Numer. Model.: Electron. Netw. Devices Fields **33** (2020), no. 1, e2686.
[31] F. Usta, M. Akyiğit, F. Say, and K.J. Ansari, *Bernstein operator method for approximate solution of singularly perturbed Volterra integral equations*, J. Math. Anal. Appl. **507** (2022), no. 2, 125828.
[32] M. Izadi, *Two-stage explicit schemes based numerical approximations of convection-diffusion equations*, Int. J. Comput. Sci. Math. **16** (2022), no. 3, 208–224.
[33] H. Delannoy, *Emploi de Íechiquier pour la resolution de certains problÂţemes de probabilites*, Assoc. Franc. Bordeaux **24** (1895), 70–90.
[34] Z. Sun, *Congruences involving generalized central trinomial coefficients*, Sci. China Math. **57** (2014), 1375–1400.
[35] Ö. K. Kürkcü, *A novel numerical implementation for solving time fractional telegraph differential equations having multiple space and time delays via Delannoy polynomial*, MANAS J. Eng. **9** (2021), no. 1, 82–96.
[36] E. D. Rainville, *Special Functions*, Macmillan, New York, 1960.
[37] E. Rothe, *Zweidimensionale parabolische randwertaufgaben als grenzfall eindimensionaler randwertaufgaben*, Math. Ann. **102** (1930), no. 1, 650–670.
[38] H. M. Srivastava and M. Izadi, *The Rothe-Newton approach to simulate the variable coefficient convection-diffusion equations*, J. Mahani Math. Res. **11** (2022), no. 2, 141–157.
[39] M. Izadi and P. Roul, *Spectral semi-discretization algorithm for a class of nonlinear parabolic PDEs with applications*, Appl. Math. Comput. **429** (2022), 127226.
[40] M. Izadi and M. E. Samei, *Time accurate solution to Benjamin-Bona-Mahony Burgers equation via Taylor-Boubaker series scheme*, Bound. Value Probl. 2022 (2022), 17.
[41] M. Izadi, *A combined approximation method for nonlinear foam drainage equation*, Sci. Iran. **29** (2022), no. 1, 70–78.
[42] M. H. Protter and H. F. Weinberger, *Maximum Principles in Differential Equations*, Reprint of the 1967 original, Springer-Verlag, New York, NY, 1984.